Chapter 14

Visualization of Retinoid Storage and Trafficking by Two-Photon Microscopy

Yoshikazu Imanishi and Krzysztof Palczewski

Abstract

Vertebrate vision is maintained by the retinoid (visual) cycle, a complex enzymatic pathway that operates in the retina to regenerate the visual chromophore, 11-*cis*-retinal, a prosthetic group of rhodopsin that undergoes activation by light. Many different mutations in genes encoding retinoid cycle proteins can cause a variety of human blinding diseases. Two-photon microscopy is an evolving, non-invasive, and repetitive imaging technology that can be used to monitor biomolecules within the vertebrate retina at a subcellular resolution. This method has the great advantage of portraying endogenous retinoid fluorophores in their native state without the need for artificial staining. Such real-time retinal imaging permits rapid evaluation not only of various stages of retinal disease in live animal models of human retinopathies but also of the outcome from intended pharmacological therapies. Two-photon microscopy offers substantial potential for early detection of age- and disease-related changes in the eye, long before clinical or pathological manifestations become apparent.

Key words: Rhodopsin, retinoid isomerization, retinol, two-photon microscopy, RPE, retina, lipid droplet, retinosome.

Abbreviations: The abbreviations used are as follows

HPLC	high pressure liquid chromatography
NA	numerical aperture
REST	retinyl ester storage structure (retinosome)
RPE	retinal pigmented epithelium
TPM	two-photon microscopy
UV	ultraviolet light.

1. Introduction

Retinoids are signaling molecules essential for a number of biological processes including development, immunity, and vision. One active form of retinoids, 11-*cis*-retinal, is the chromophore

H. Sun, G.H. Travis (eds.), *Retinoids*, Methods in Molecular Biology 652,
DOI 10.1007/978-1-60327-325-1_14,

of rhodopsin and cone visual pigments (1). For each photon absorbed by rhodopsin, a single molecule of 11-*cis*-retinal is converted to all-*trans*-retinal. Since retinoids cannot be synthesized in the body, they must be derived from dietary sources. Dietary retinoids are temporarily stored as retinyl esters, primarily in liver, and then used to generate active retinoid species, including 11-*cis*-retinal. To maximize their usage of retinoids, eyes have evolved a unique recycling mechanism for the replenishment of visual pigment chromophores during continuous illumination. Conversion of all-*trans* back to 11-*cis*-retinal requires a series of biochemical reactions occurring in the photoreceptors and subsequently in the retinal pigmented epithelium (RPE) (2, 3). The cycle of reactions required for the regeneration of 11-*cis*-retinal is called the retinoid (or visual) cycle, and deficiencies in its components can lead to a variety of blinding disorders (4, 5). Among the retinoid intermediates of the cycle, fatty acid all-*trans*-retinyl esters are key substrates for an isomerase RPE65. From all-*trans*-retinyl esters, RPE65 generates 11-*cis*-retinol (6–8), which then is oxidized to 11-*cis*-retinal by retinol dehydrogenases (9–11). Since only the RPE is capable of generating 11-*cis*-retinoids, efficient trafficking of retinoids between photoreceptor cells and the RPE is required to complete the retinoid cycle. Currently, studies of the retinoid cycle largely depend on high pressure liquid chromatography (HPLC)-based assays (12). Although HPLC is an excellent tool for quantification and identification of retinoid compounds, it lacks the spatiotemporal resolution essential for understanding their metabolism and trafficking in a subcellular structural context.

To study directly the roles of retinoid trafficking in vision, we sought a methodology to monitor retinoid flow in intact mouse eyes at a resolution conferred by fluorescence microscopy (<1 μm). Intrinsic fluorescence of retinols and retinyl esters is often used in analytical chemistry to identify different retinoid species (12). However, the drawback of fluorescent imaging of retinol and retinyl esters, from a biological standpoint, is that the excitation light required for their activation lies in the ultraviolet (UV) range (~325 nm). Short-wavelength UV light is prone to scatter and get absorbed by biological molecules, resulting in less efficient excitation especially in thick (50–200 μm) biological tissue samples. Also, large doses of UV light can destroy cells and may cause cataracts in the lens. To circumvent these unfavorable properties, we introduced the application of two-photon microscopy (TPM) (*see* **Note 1**), in which excitation of a fluorophore is accomplished by nearly simultaneous absorption of two photons in the infrared region (13). Infrared light as used in TPM is considered less toxic and can penetrate tissues better than UV light (14–16). TPM, similar to confocal microscopy, permits monitoring of three-dimensional distributions of fluorescent

molecules. But in contrast to confocal microscopy, excitation of molecules in TPM is limited within a focal spot of less than 1 fl volume (17). Because of this highly localized two-photon excitation, optical sectioning is possible by scanning specimens, without a confocal pinhole in front of the photon detectors.

Both for TPM and other conventional microscopes, high-resolution imaging requires the use of a high numerical aperture (NA) objective lens. Just as important, the efficacy of two-photon excitation is dependent on the fourth power of the NA (18), so the signal-to-noise ratio improves dramatically by using an objective lens with a higher NA. However, high NA lenses generally have short working distances and cannot reach deep inside a specimen. We found that two-photon imaging of the RPE can be accomplished by applying short-pulsed illumination through the sclera and the choroid of mouse eyes (**Fig. 14.1A**). Under these imaging conditions and with the involved target geometry, the working distance can be kept as short as 50–100 μm to reach the RPE layer. By taking advantage of this short distance, we successfully applied an objective lens with a NA ranging from 0.7 to 1.3 to imaging the RPE of mouse eyes.

TPM with excitation at ~730 nm was applied to RPE cells *ex vivo* to learn how fatty acid retinyl esters are organized in these cells (**Fig. 14.1B**, **a**). The emission signal was collected

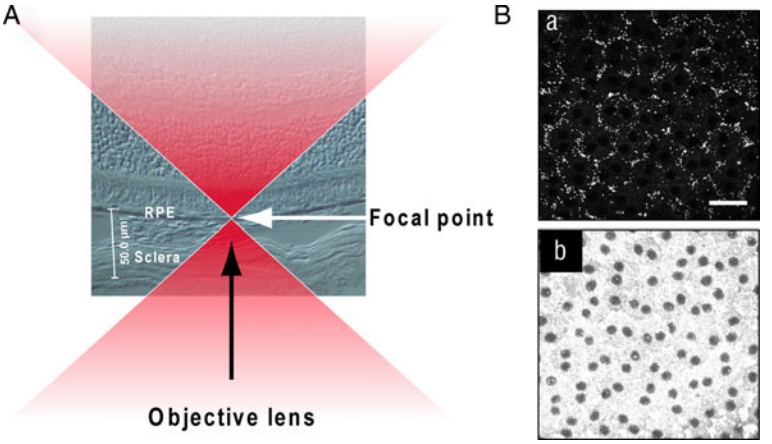

Fig. 14.1. Transscleral imaging of mouse RPE. (**A**) A diagram illustrating the use of transscleral two-photon imaging to study the RPE and retina. Non-pigmented mouse eyes need to be used for this application. The objective lens is located proximal to the surface of the sclera. The *black arrow* indicates the direction of the excitation light. Because of the short distance between the objective lens and the RPE cells, high-resolution imaging is possible with a high NA lens. (**B**) Imaging of retinyl ester fluorescence in the RPE of isolated mouse eyes. At low-power two-photon excitation (*top image*), retinyl ester storage structures are visible proximal to plasma membranes. At high-power two-photon excitation (*bottom image*), less abundant diffusively located retinoids become visible. Nuclei do not show a fluorescence signal, suggesting that retinoids localize to the cytoplasmic area. *Top and bottom images* were collected from the same group of RPE cells. Scale bar, 20 μm.

through a custom-made bandpass filter (HQ 465/160, Chroma Technology Corp., Rockingham, VT) to monitor fluorescence in the 385–545 nm range. Previous studies indicated that fatty acid retinyl esters are compartmentalized in small subcellular structures we named retinyl ester storage structures (RESTs, also called retinosomes) (19) that were visualized by excitation at an intensity of ~3 mW (**Fig. 14.1B**, **a**). Additional diffuse fluorescence in the cytoplasmic area was noted after increasing the excitation intensity to ~30 mW (**Fig. 14.1B**, **b**), suggesting that the observed fluorescence originates from retinyl esters. To identify the molecular origin of the observed fluorescence, we compared the fluorescence changes in subcellular structures before (**Fig. 14.2A**, **a**) and after (**Fig. 14.2A**, **b**) application of all-*trans*-retinol to the RPE cells. Not only was an increase of fluorescence observed in the RPE cells (**Fig. 14.2A**, **c**) but it also correlated with an increased level of all-*trans*-retinyl esters found in the specimen (**Fig. 14.2A**, **d**). In conjunction with the lack of RPE fluorescence in mice deficient in the formation of retinyl esters (19), we conclude that the fluorescence seen in the RPE mainly originates from retinyl esters.

Two-photon retinyl ester imaging can be combined with immunofluorescence confocal microscopy. Localization of all-*trans*-retinyl esters was stable after fixation with 4% paraformaldehyde for 30 min and subsequent incubation in the presence of

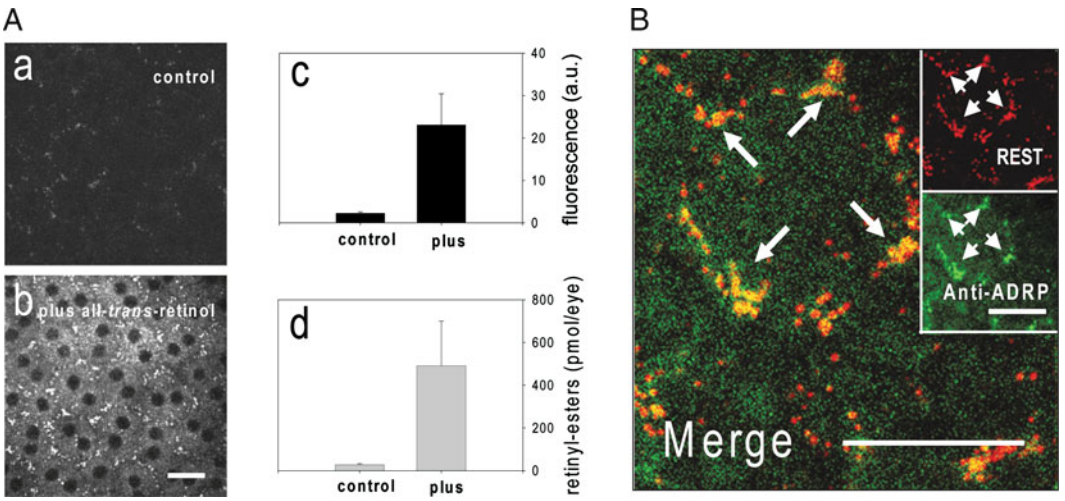

Fig. 14.2. Studies of retinyl ester storage structures (RESTs). (**A**) (**a**) RPE cells in an eyecup preparation. (**b**) RPE cells in an eyecup preparation after application of all-*trans*-retinol. Newly formed all-*trans*-retinyl esters localized into the RESTs. (**c**) Fluorescence in the RPE quantified before and after treatment with all-*trans*-retinol. Fluorescence increased after the treatment. (**d**) All-*trans*-retinyl esters in the eyecups quantified before and after treatment with all-*trans*-retinol. All-*trans*-retinyl esters increased after treatment. (**B**) Two-photon imaging of RESTs reveals colocalization of Adfp. Adfp (*green* fluorescence) specifically localized to the RESTs (*red* fluorescence) as shown by *yellow* color in the merged image. Adapted from Imanishi et al. (19). Scale bars, 20 μm. This research was originally published in the *Journal of Cell Biology* (19). The Rockefeller University Press.

0.1% Triton X-100 for over 3 h. Because of this stability, eyecups can be processed for immunofluorescence staining without compromising the arrangement of RESTs. **Figure 14.2B** indicates the localization of adipose differentiation-related protein (Adfp) (20), a component frequently found on lipid droplets. Adfp (**Fig. 14.2B**, green color) co-localized with RESTs (**Fig. 14.2B**, red color) in the RPE cells, suggesting its interaction with retinyl esters. As indicated by the example of Adfp, this type of combined analysis is especially useful for discovering new components of RESTs.

The most advantageous capability of TPM is monitoring retinyl ester dynamics in vivo. In this regard, the described application provides an advantage over previously published methods for imaging retinoids. In the 1980s, Kaplan introduced UV-excitation fluorescence microscopy to monitor formation of all-*trans*-retinol after photobleaching rhodopsin (21). More recently, Koutalos and his colleagues used a more sensitive fluorescence microscope to monitor the in situ formation and diffusion of all-*trans*-retinol in photoreceptor outer segments (22–24). However, all of these studies were performed on isolated photoreceptor segments or retina slices that lack photoreceptor–RPE contacts. An intact photoreceptor–RPE interface is essential for the proper transport of all-*trans*-retinol from photoreceptors to RPE cells. These contacts are maintained in either isolated eyes or anesthetized mice used for our studies. In an anesthetized mouse (**Fig. 14.3A**), transport and subsequent incorporation of retinoid from photoreceptors into the RPE cells can be documented (**Fig. 14.3B**). Immediately after photoactivation of rhodopsin (**Fig. 14.3B**, left), RESTs showed relatively weak fluorescence. However, 30 min after photoactivation (**Fig. 14.3B**, right), RESTs showed strong fluorescence. Retinyl ester levels increased in the RPE due to formation of all-*trans*-retinol in photoreceptors, trafficking of all-*trans*-retinol to the RPE, and esterification of all-*trans*-retinol by lecithin-retinol acyltransferase (19, 25). The increase of the fluorescence showed a time course similar to the increase of retinyl esters in vivo, indicating that the RPE cells were functional during this imaging procedure (19).

Two-photon imaging of RPE is not just limited to mouse models but also is applicable to other species including humans. A human RPE layer was fixed after removing the retina from an eyecup, and the RPE layer was dissected out along with the choroid layer. Small pieces (<1 cm^2) of tissue then were mounted on glass-bottomed 35-mm dishes (MatTek Corp.). RPE cells corresponding to the locations 1–4 shown in **Fig. 14.4A** were imaged under the same conditions. In the area proximal to the edge of retina (**Fig. 14.4B**, **1**), RPE cells had irregular shapes and punctate fluorescent structures were observed throughout these cells. In equatorial, macular, and foveal regions (**Fig. 14.4B**,

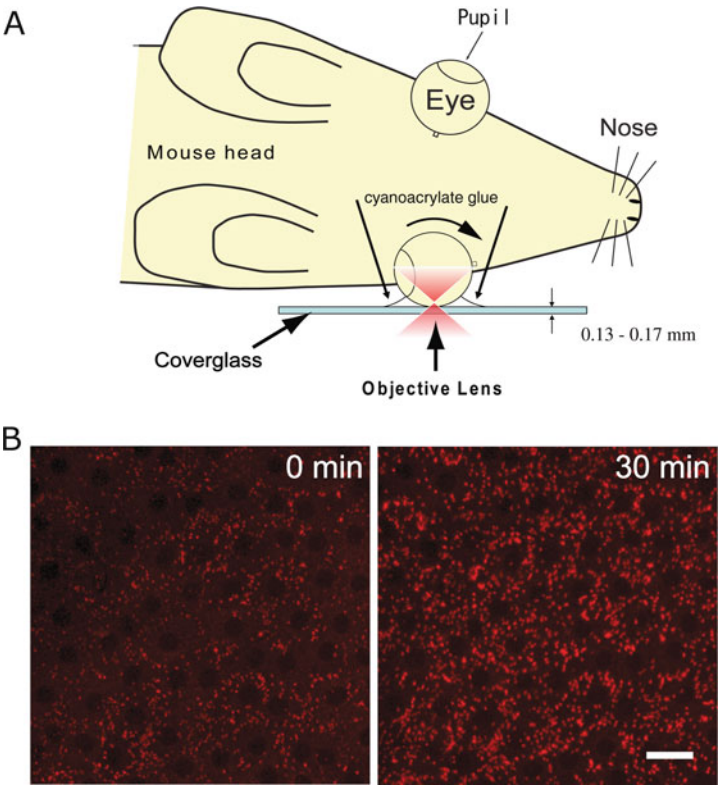

Fig. 14.3. Two-photon imaging of RPE cells in vivo. (**A**) A diagram illustrating two-photon imaging of mouse RPE cells in vivo. One eye of an anesthetized mouse is rotated to image the peripheral part of the RPE layer and the eye is immobilized on a coverglass with cyanoacrylate glue. An infrared short pulse laser beam (in *red color*) is passed through the sclera and focused on the RPE. (**B**) RPE cells in the peripheral region imaged by TPM. Retinyl ester fluorescence was imaged at 0 min (*left*) and 30 min (*right*) after rhodopsin stimulation by light. Retinyl ester fluorescence increased at 30 min. Images are adapted and modified from Imanishi et al. (25). Scale bar, 20 μm. This research was originally published in the *Journal of Biological Chemistry* (25). © The American Society for Biochemistry and Molecular Biology.

2–4), these fluorescent structures were arranged in a more orderly fashion proximal to the border of RPE cells. Considerable variation in absolute fluorescence intensities was observed amongst the eye specimens tested, irrespective of the subject's age. However, the macular RPE always exhibited the highest fluorescence intensities in each eye, whereas the equatorial and foveal RPE showed about threefold weaker fluorescence intensities (**Fig. 14.4C**). The macular region contains the highest density of photoreceptors (26) so this result is consistent with the high densities of retinoids in the macular region of primate eyes (27).

Studies of RESTs should provide a new avenue for understanding the link between lipid storage and the retinoid cycle (19). Methods described in **Section 3.4** (**Fig. 14.2**) will allow identification of novel REST components whereas the method in

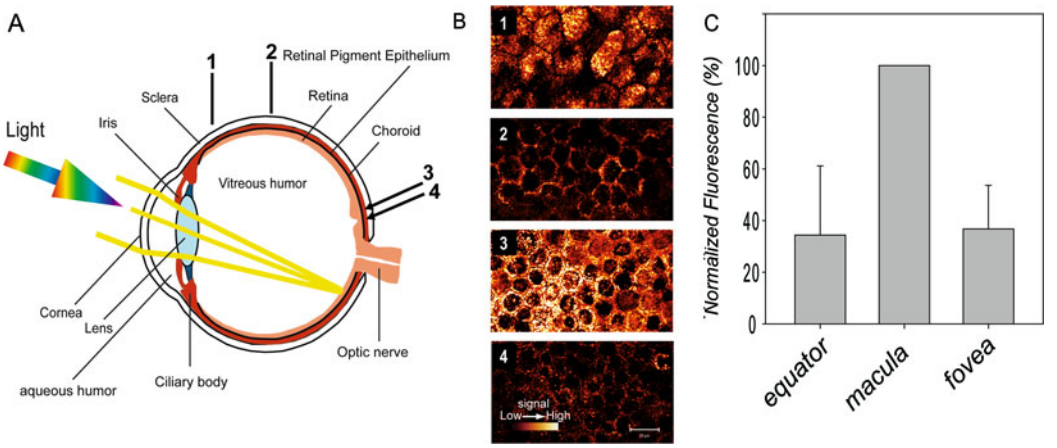

Fig. 14.4. Imaging of human RPE by two-photon microscopy. (**A**) Schematic drawing of a cross section of human eye. *Arrows* with numbers 1–4 indicate locations of RPE imaged by TPM. (**B**) Two-photon imaging of human RPE cells. Retinosome-like structures can be seen proximal to the plasma membrane. (**C**) Relative fluorescence intensities measured at different regions of four human eyes. Fluorescence intensities in the equator (position 2 in **A**) and fovea (position 4 in **A**) were normalized to intensities in the macula. Scale bar, 20 μm.

Section 3.5 (**Fig. 14.3**) can be used to study the storage and trafficking of retinyl esters in animal models deficient in REST components. One REST component examined in this manner, Adfp protein, was found to be involved in the storage and trafficking of retinyl esters in the RPE (25). Another application with far-reaching implications is the use of TPM for the diagnosis of diseases caused by dysfunction of RPE cells. Involved diseases include, but may not be limited to, retinitis pigmentosa, Leber's congenital amaurosis, cone–rod dystrophy, and macular degeneration. In mice with deficiencies in the retinoid cycle, obvious changes in either the dynamics or fluorescence intensities of RESTs were observed (19, 28). Thus it will be interesting to apply the TPM method in **Section 3.6** (**Fig. 14.4**) to RPE cells isolated from patients with inherited eye diseases. Such studies will allow us to monitor how the disease affects normal retinoid metabolism of RPE cells. In the future, it would be desirable to develop a two-photon imaging technology for non-invasive imaging of living human eyes. This would expedite following age-dependent changes of retinoid metabolism in the same individual over time, a technology especially useful for studying progressive retina diseases. Imaging technologies are currently under intense development to visualize structures in the living human eye; most notably, photoreceptors can be resolved by introducing adaptive optics into an ophthalmoscope (29). Furthermore, the combination of adaptive optics and TPM can increase both resolution and signal intensity (30). With continuing innovation, we envision that two-photon imaging of the retina will play a pivotal role in studying the retinoid cycle, both in basic and in clinical research.

2. Materials

Unless otherwise noted, all named reagents are available for purchase from either Fisher Scientific (Pittsburgh, PA) or Sigma-Aldrich (St. Louis, MO).

1. Balb/c mice (Jackson Laboratory, Bar Harbor, ME). Obtain IACUC approval for experimental use of mice.
2. Dissection tools: Spring scissors (catalog no. 15017-10 and 15004-08, Fine Science Tools Inc., Foster City, CA), tweezers (catalog no. 11252-30, Fine Science Tools Inc., Foster City, CA), no. 11 Surgical blades (Becton Dickinson, Franklin Lakes, NJ).
3. A glass-bottomed 35-mm dish (Mattek Corporation, Ashland, MA).
4. Ames medium: Powder of Ames medium (Sigma-Aldrich). Dissolve 8.8 g of powder in 1 l of distilled H_2O. Add 1.9 g of sodium bicarbonate to the medium. Equilibrate with 95% O_2 and 5% CO_2.
5. All-*trans*-retinol: Dissolve all-*trans*-retinol in Ames medium containing 100 mM (2-hydroxypropyl)-β-cyclodextrin with vigorous vortex mixing.
6. Paraformaldehyde (4%): Powder of paraformaldehyde (EM sciences, Hatfield, PA). Prepare 4% solution in 0.1 M phosphate buffer (100 mM sodium phosphate, pH 7.4).
7. PBS: 136 mM NaCl, 11.4 mM sodium phosphate, 0.1% Triton X-100, adjusted to pH 7.4.
8. PBST: PBS with 0.1% Triton X-100.
9. Blocking solution: PBST with 1.5% goat serum.
10. Antibodies: Primary antibody – Guinea pig anti-Adfp (Progen, Heidelberg, Germany). Secondary antibody – Cy2-conjugated donkey anti-guinea pig IgG (Jackson ImmunoResearch Laboratories, Inc., West Grove, PA). Dilute antibodies in PBST at concentrations recommended by the vendors.
11. No. 1 Safelight filter (Eastman Kodak, Rochester, NY).
12. Ketamine and xylazine mixture: Mix to final concentrations of 6 mg/ml ketamine (Bioniche Pharma Inc., Bogart, GA), 0.44 mg/ml xylazine, 10 mM phosphate buffer, and 100 mM NaCl in distilled H_2O. Adjust pH to 7.4.
13. Cyanoacrylate glue from Elmer's Products Inc. (Columbus, OH).
14. Scotch tape (3 M Corporate, St. Paul, MN).
15. Circular cover glass (44-mm diameter, 0.16-mm thickness) (Carl Zeiss MicroImaging Inc., Thornwood, NY).

16. A flash unit (Nikon, Melville, NY).
17. Human eyes, 8–12-h postmortem, obtained through Lions Eye Bank (Seattle, WA). Legal requirements for use of human donor retinas and primate retinas should be met (University of Washington Human Subjects, approval on file).

3. Methods

3.1. Configurations of Two-Photon Microscopes and Imaging Procedures

To obtain the data shown in **Figs. 14.2** and **14.4**, perform TPM with a Zeiss LSM 510 MP-NLO confocal microscope (Carl Zeiss, Germany) with LSM 510 software 3.0. Focus laser pulses of 730 nm from a mode-locked Ti:sapphire laser, Mira-900 (Coherent, Mountain View, CA) on the RPE through the sclera with a Plan-Neofluar 40×/1.3NA objective lens (Carl Zeiss). Alternatively, to obtain the data in **Figs. 14.1B** and **14.3**, perform two-photon excitation microscopy with a Leica TCS SP2 scanning head (Leica) attached to a DM IRBE2 inverted microscope (Leica Microsystems Inc., Bannockburn, IL). Use LCS 3D Software (Leica, Germany) for data acquisition. Deliver laser pulses of 730 nm from a mode-locked Ti:sapphire laser, Chameleon^{TM}-XR (Coherent, Mountain View, CA), through the microscope system to the RPE through the sclera with an HCX PL APO 40× oil immersion objective lens (NA= 1.25, Leica) (*see* **Note 2**).

For both the microscope systems, maintain the reaction temperature at 36–37°C using a temperature-controlled microscope stage (Heating insert P and Tempcontrol 37-2, PeCon, Erbach, Germany). Maintain 40× objective lenses at 37°C with an objective heater (PeCon) or an ASI 400 air stream incubator (NEVTEK, Williamsville, VA) (*see* **Note 3**). Collect sample fluorescence (385–545 nm) through the objective lens, separated from the excitation light by a dichroic mirror, and filter fluorescence through custom-made filters (HQ 465/160, Chroma Technology Corp., Rockingham, VT) and direct it to a photomultiplier tube detector. Photomultiplier tube detectors should be installed in a non-descanned detection configuration, in which the fluorescence emission is directly delivered to the detectors without passing through the X–Y scanner (*see* **Note 4**). Measure the laser beam intensity at the back aperture of the objective lens and keep it at 3–30 mW for ex vivo studies and ~5 mW for in vivo studies. The imaging resolution should be 0.22–0.24 μm/pixel for ex vivo studies (**Figs. 14.1**, **14.2**, and **14.4**) and 0.44 μm/pixel for in vivo studies (**Fig. 14.3**). Set the line scanning rate at 400 Hz.

3.2. Two-Photon Imaging of RPE Cells in Mouse Eyeball Preparations

1. After euthanasia, dissect out a mouse eyeball with spring scissors and tweezers (*see* **Note 5**).
2. Locate the eyeball at the center of a 35-mm glass-bottomed dish with the sclera in direct contact with the coverslip at the bottom of the dish. Keep the eyeball hydrated with Ames medium.
3. Place the 35-mm dish on the microscope stage.
4. Collect images as described in **Section 3.1**.

3.3. Two-Photon Imaging of RPE in Mouse Eyecup Preparations

1. After euthanasia, dissect out a mouse eyeball with spring scissors and tweezers. Place the eyeball in a Petri dish and wash with Ames medium.
2. To remove the cornea, cut ~0.5 mm below the corneal limbus with a number 11 surgical blade and spring scissors. Remove the lens and retina with fine tweezers and spring scissors. Dissect the eye in fresh Ames medium. After dissection, the RPE should be exposed to the Ames medium (*see* **Notes 6** and **7**).
3. Locate the eyecup at the center of a glass-bottomed 35-mm dish (MatTek Corporation, MA) so that the sclera is in direct contact with the coverslip at the bottom of the dish.
4. Apply a drop (20–50 μl) of fresh Ames medium onto the RPE. Prevent eyecup from floating by adjusting the volume of added fluid (*see* **Note 8**).
5. Image the RPE by TPM as explained in **Section 3.1**.
6. Remove Ames medium and apply a drop (20–50 μl) of 1.4 mM all-*trans*-retinol to the RPE. After 3 min, gently remove the solution and wash the eyecup with Ames medium. Collect an image by TPM as described in **Section 3.1**.
7. Obtain images from the RPE before and after all-*trans*-retinol treatment as shown in **Fig. 14.2A**.

3.4. Two-Photon and Confocal Imaging of the RPE to Discover Protein Components of Retinyl Ester Storage Structures

1. Isolate a mouse eyecup by following the procedures in **Section 3.3**.
2. Gently apply 1 ml of 4% paraformaldehyde onto the eyecup preparation.
3. Fix the tissue for 30 min.
4. Remove the paraformaldehyde and wash the eyecup with 1 ml of PBST. Wash three times for 5 min each.
5. Remove PBST and incubate the eyecup in 1 ml of blocking solution. Incubate at room temperature for 15 min.
6. Remove blocking solution and add 100 μl of primary antibody diluted in PBST solution. If a sufficient amount of primary antibody is available, increase the volume (*see* **Note 9**).

7. Wash the eyecup with 1 ml of PBST three times for 5 min each.
8. Remove PBST and apply 500 μl of diluted secondary antibody.
9. Incubate for 30–45 min and then wash the eyecup with 1 ml of PBST three times for 5 min each.
10. Locate the eyecup at the center of a glass-bottomed 35-mm dish (MatTek Corporation, MA) so the sclera is in direct contact with the bottom coverslip.
11. Find the RPE cell layer by scanning the eye sample in XYZ directions by two-photon microscopy.
12. Collect an image of retinyl ester storage structures by following the procedure in **Section 3.1**.
13. Then collect an immunofluorescence image by using the filter, a dichroic mirror, and laser beam appropriate for the fluorescent molecule conjugated with the secondary antibody (*see* **Note 10**).

3.5. Two-Photon Imaging of RPE Cells in a Live Mouse

1. Maintain mice in the dark (>1 week) before the experiment (*see* **Note 11**).
2. Perform all the procedures under a safelight (>560 nm).
3. Anesthetize a mouse by intraperitoneal injection of the ketamine/xylazine mixture at a dose of 15 μl/g body weight (*see* **Note 12**).
4. Maintain the mouse at 36–37°C until the anesthesia becomes deep enough for the experiment.
5. Apply a small amount of cyanoacrylate glue between the eye and cover glass (*see* **Fig. 14.3A**) (*see* **Note 13**).
6. Lay the mouse on the microscope stage maintained at 36–37°C. Mount the cover glass on the stage and immobilize it by using scotch tape.
7. Find the RPE cell layer by scanning the eye sample in XYZ directions by two-photon microscopy (*see* **Section 3.1**).
8. Obtain an image of the RPE by two-photon microscopy as described in **Section 3.1**.
9. Expose the eye to intense light flashes to bleach ~60% of the visual pigment.
10. Image the RPE cells every 1–10 min as described in **Section 3.1**.

3.6. Two-Photon Imaging of the RPE from a Human Eye

1. Fix a human eyeball in 20 ml of 4% paraformaldehyde for 10 min (*see* **Note 14**).
2. Place the eyeball into a Petri dish with PBS.

3. Remove the lens, cornea, vitreous, and retina from the eye to prepare an eyecup (*see* **Note 15**).
4. Fix the eyecup in 20 ml of 4% paraformaldehyde for 1 h.
5. Wash the eyecup with 20 ml of PBS three times for 5 min each.
6. With the eyecup, peel the RPE along with the choroid off the sclera.
7. Cut the RPE/choroid layer into 1 × 1 cm squares; obtain tissue pieces from regions 1–4 as shown in **Fig. 14.4A**. RPE cells from the macular region are readily discerned because they are more deeply pigmented than cells within the peripheral regions.
8. Place the samples on a 35-mm glass-bottomed dish so that the RPE cells directly contact the surface of the glass and the choroid faces toward the top.
9. Apply two-photon imaging as described in **Section 3.1**.
10. For quantification of fluorescence, use the "measure" function in ImageJ software. Normalized pixel values for different areas of the retina are compared in **Fig. 14.4C**. Pixel values should be averaged for entire image fields. Intensities in the nucleus should be used as background and subtracted from measured values.

4. Notes

1. Two-photon microscopy, used throughout this manuscript, is a broad term that includes two-photon excitation laser scanning microscopy and second harmonic imaging microscopy.
2. When using an oil or a water immersion objective lens on an inverted microscope, the diameter of the immersion fluid is a good indicator for estimating the distance between the objective lens and the bottom of the dish. When starting each imaging session, adjust the location of the objective lens as close as possible to the bottom of the dish.
3. The objective lens is a large heat sink. So when used, it needs to be warmed to the physiological temperature of an animal or tissue.
4. Non-descanned detection is highly sensitive and affected by light from computer monitors and other sources. Therefore, we recommend turning off room lighting. Also, do not use the mercury lamp and halogen lamp of the microscope system. We found that the noise level can be reduced

by covering the computer monitors with red filter sheets (E-color, Rosco Laboratories Inc., Stamford, CT).

5. Pigmented mice are not well suited for imaging through the sclera so albino Balb/c mice were primarily used for our studies. Another commonly used strain, the C57BL/6, tyrosinase mutant mouse (Tyr^{c-2J}), is not pigmented and is available from Jackson Laboratories (Bar Harbor, ME).
6. In **Section 3.3**, we found it difficult to penetrate RPE cells with all-*trans*-retinol if the retina is attached to the RPE. Similar difficulties were encountered in applying several reagents, including FM4-64, BODIPY FL C_5-ceramide, MitoTracker Orange CMTMRos, LysoTracker Green DND-26, $DiOC_6$, and Nile Red (Invitrogen Corporation, Carlsbad, CA). Thus, it is essential to remove the retina to test the effect of small test molecules on the RPE cell layer.
7. In **Sections 3.3** and **3.4**, it is easier to access the retina if an eye is cut ~0.5 mm below the corneal limbus to remove the cornea first.
8. In **Sections 3.3** and **3.4**, the RPE layer an eyecup preparation is fragile so all solutions should be applied gently.
9. Before proceeding to the procedure in **Section 3.4**, confirm that the primary antibody works on cryosections of mouse eye when viewed by the same detection method (e.g., Alexa 488 or Cy3-labeled secondary antibodies).
10. In **Section 3.4**, misalignment of confocal and TPM lasers will result in a shift of two channels of the merged images. Ask the microscope vendor or laser specialist to align the lasers precisely.
11. In **Section 3.5**, this in vivo imaging method is applicable only to the peripheral part of the retina, because the central part of the eye is embedded in the orbital cavity and inaccessible. In the peripheral part of the retina (**Fig. 14.3**), we recognize that retinyl ester storage structures are less organized than those in the central retina (**Fig. 14.1B**). Disorganized fluorescent structures are found at the edge of the human retina as well (**Fig. 14.4B**).
12. In **Section 3.5**, individual differences were observed in the susceptibility of mice to the anesthesia. Monitor the condition of these animals carefully during the imaging procedure.
13. In **Section 3.5**, we noticed that the eyes are embedded deeper in the orbital cavity of older mice. For in vivo imaging, the RPE is optically more accessible in young mice (3–4 weeks) than in older mice (>months).

14. In **Section 3.6**, human eyes are a potential source of blood-borne pathogens. Comply with OSHA regulations for handling potential sources of blood-borne pathogens. Upon receipt of these eyes, place them immediately in 4% paraformaldehyde.
15. In **Section 3.6**, to facilitate removal of the human retina, remove the cornea and lens by cutting 2–3 mm below the corneal limbus.

Acknowledgments

This research was supported in part by grants EY009339 and P30 EY11373 from the National Institutes of Health and the Foundation Fighting Blindness.

References

1. Palczewski, K. (2006) G protein-coupled receptor rhodopsin. *Annu. Rev. Biochem.* **75**, 743–767.
2. McBee, J.K., Palczewski, K., Baehr, W., Pepperberg, D.R. (2001) Confronting complexity: The interlink of phototransduction and retinoid metabolism in the vertebrate retina. *Prog. Retin. Eye Res.* **20**, 469–529.
3. Lamb, T.D., Pugh, E.N., Jr. (2004) Dark adaptation and the retinoid cycle of vision. *Prog. Retin. Eye Res.* **23**, 307–380.
4. Thompson, D.A., Gal, A. (2003) Vitamin A metabolism in the retinal pigment epithelium: Genes, mutations, and diseases. *Prog. Retin. Eye Res.* **22**, 683–703.
5. Travis, G.H., Golczak, M., Moise, A.R., Palczewski, K. (2007) Diseases caused by defects in the visual cycle: Retinoids as potential therapeutic agents. *Annu. Rev. Pharmacol. Toxicol.* **47**, 469–512.
6. Moiseyev, G., Chen, Y., Takahashi, Y., Wu, B.X., Ma, J.X. (2005) RPE65 is the isomerohydrolase in the retinoid visual cycle. *Proc. Natl. Acad. Sci. USA* **102**, 12413–12418.
7. Jin, M., Li, S., Moghrabi, W.N., Sun, H., Travis, G.H. (2005) Rpe65 is the retinoid isomerase in bovine retinal pigment epithelium. *Cell* **122**, 449–459.
8. Redmond, T.M., Poliakov, E., Yu, S., Tsai, J.Y., Lu, Z., Gentleman, S. (2005) Mutation of key residues of RPE65 abolishes its enzymatic role as isomerohydrolase in the visual cycle. *Proc. Natl. Acad. Sci. USA* **102**, 13658–13663.
9. Yamamoto, H., Simon, A., Eriksson, U., Harris, E., Berson, E.L., Dryja, T.P. (1999) Mutations in the gene encoding 11-*cis* retinol dehydrogenase cause delayed dark adaptation and fundus albipunctatus. *Nat. Genet.* **22**, 188–191.
10. Driessen, C.A., Winkens, H.J., Hoffmann, K., Kuhlmann, L.D., Janssen, B.P., Van Vugt, A.H., Van Hooser, J.P., Wieringa, B.E., Deutman, A.F., Palczewski, K., Ruether, K., Janssen, J.J. (2000) Disruption of the 11-*cis*-retinol dehydrogenase gene leads to accumulation of *cis*-retinols and *cis*-retinyl esters. *Mol. Cell. Biol.* **20**, 4275–4287.
11. Kim, T.S., Maeda, A., Maeda, T., Heinlein, C., Kedishvili, N., Palczewski, K., Nelson, P.S. (2005) Delayed dark adaptation in 11-*cis*-retinol dehydrogenase-deficient mice: A role of RDH11 in visual processes in vivo. *J. Biol. Chem.* **280**, 8694–8704.
12. Saari, J.C., Garwin, G.G., Haeseleer, F., Jang, G.F., Palczewski, K. (2000) Phase partition and high-performance liquid chromatography assays of retinoid dehydrogenases. *Methods Enzymol.* **316**, 359–371.
13. Denk, W., Strickler, J.H., Webb, W.W. (1990) Two-photon laser scanning fluorescence microscopy. *Science* **248**, 73–76.
14. Denk, W., Svoboda, K. (1997) Photon upmanship: Why multiphoton imaging is more than a gimmick. *Neuron* **18**, 351–357.
15. Svoboda, K., Yasuda, R. (2006) Principles of two-photon excitation microscopy and its applications to neuroscience. *Neuron* **50**, 823–839.

16. Imanishi, Y., Lodowski, K.H., Koutalos, Y. (2007) Two-photon microscopy: Shedding light on the chemistry of vision. *Biochemistry* **46**, 9674–9684.
17. Williams, R.M., Piston, D.W., Webb, W.W. (1994) Two-photon molecular excitation provides intrinsic 3-dimensional resolution for laser-based microscopy and microphotochemistry. *FASEB J.* **8**, 804–813.
18. Diaspro, A. (ed.). (2002) *Confocal and Two-Photon Microscopy: Foundations, Applications, and Advances*, Wiley-Liss, New York, NY.
19. Imanishi, Y., Batten, M.L., Piston, D.W., Baehr, W., Palczewski, K. (2004) Noninvasive two-photon imaging reveals retinyl ester storage structures in the eye. *J. Cell. Biol.* **164**, 373–383.
20. Jiang, H.P., Serrero, G. (1992) Isolation and characterization of a full-length cDNA coding for an adipose differentiation-related protein. *Proc. Natl. Acad. Sci. USA* **89**, 7856–7860.
21. Kaplan, M.W. (1985) Distribution and axial diffusion of retinol in bleached rod outer segments of frogs (*Rana pipiens*). *Exp. Eye Res.* **40**, 721–729.
22. Cornwall, M.C., Tsina, E., Crouch, R.K., Wiggert, B., Chen, C., Koutalos, Y. (2003) Regulation of the visual cycle: Retinol dehydrogenase and retinol fluorescence measurements in vertebrate retina. *Adv. Exp. Med. Biol.* **533**, 353–360.
23. Chen, C., Tsina, E., Cornwall, M.C., Crouch, R.K., Vijayaraghavan, S., Koutalos, Y. (2005) Reduction of all-*trans* retinal to all-*trans* retinol in the outer segments of frog and mouse rod photoreceptors. *Biophys. J.* **88**, 2278–2287.
24. Wu, Q., Chen, C., Koutalos, Y. (2006) All-*trans* retinol in rod photoreceptor outer segments moves unrestrictedly by passive diffusion. *Biophys. J.* **91**, 4678–4689.
25. Imanishi, Y., Sun, W., Maeda, T., Maeda, A., Palczewski, K. (2008) Retinyl ester homeostasis in the adipose differentiation-related protein-deficient retina. *J. Biol. Chem.* **283**, 25091–25102.
26. Rodieck, R.W. (1998) *The First Steps in Seeing*, Sinauer Associates, Inc., Sunderland, MA.
27. Jacobson, S.G., Aleman, T.S., Cideciyan, A.V., Heon, E., Golczak, M., Beltran, W.A., Sumaroka, A., Schwartz, S.B., Roman, A.J., Windsor, E.A., Wilson, J.M., Aguirre, G.D., Stone, E.M., Palczewski, K. (2007) Human cone photoreceptor dependence on RPE65 isomerase. *Proc. Natl. Acad. Sci. USA* **104**, 15123–15128.
28. Maeda, A., Maeda, T., Imanishi, Y., Golczak, M., Moise, A.R., Palczewski, K. (2006) Aberrant metabolites in mouse models of congenital blinding diseases: Formation and storage of retinyl esters. *Biochemistry* **45**, 4210–4219.
29. Roorda, A., Williams, D.R. (1999) The arrangement of the three cone classes in the living human eye. *Nature* **397**, 520–522.
30. Rueckel, M., Mack-Bucher, J.A., Denk, W. (2006) Adaptive wavefront correction in two-photon microscopy using coherence-gated wavefront sensing. *Proc. Natl. Acad. Sci. USA* **103**, 17137–17142.